NANOPHOTONICS

Few-cycle vacuum squeezing in nanophotonics

Rajveer Nehra¹+*, Ryoto Sekine¹+, Luis Ledezma^{1,2}, Qiushi Guo¹, Robert M. Gray¹, Arkadev Roy¹, Alireza Marandi^{1*}

One of the most fundamental quantum states of light is the squeezed vacuum, in which noise in one of the quadratures is less than the standard quantum noise limit. In nanophotonics, it remains challenging to generate, manipulate, and measure such a quantum state with the performance required for a wide range of scalable quantum information systems. Here, we report the development of a lithium niobate—based nanophotonic platform to demonstrate the generation and all-optical measurement of squeezed states on the same chip. The generated squeezed states span more than 25 terahertz of bandwidth supporting just a few optical cycles. The measured 4.9 decibels of squeezing surpass the requirements for a wide range of quantum information systems, demonstrating a practical path toward scalable ultrafast quantum nanophotonics.

uantum information processing offers great promise for computation, secure communication, metrology, and sensing. Many physical platforms such as nuclear spins, superconducting circuits, photonics, trapped ions, quantum dots, and neutral atoms have widely been explored in the pursuit to build quantum information processors (1). Among these, photonics stands out because of its potential for scalability, room-temperature logical operations, and ease of encoding quantum information in both discrete and continuous variables (2).

In continuous-variable (CV) quantum photonics, information is encoded in continuous amplitude and phase values of the quantized electromagnetic field. The single-mode and multimode squeezed states are widely used for various applications, including quantum-enhanced interferometry such as in the Laser Interferometer Gravitational-Wave Observatory (3), microscopy (4), and quantum teleportation (5). Moreover, highly entangled CV quantum states, that is, cluster states (6–8), serve as a universal resource for one-way quantum computation.

Typically, such high-quality CV states are generated from a single- or two-mode squeezed vacuum produced using quadratic $[\chi^{(2)}]$ parametric processes either in bulk crystals or waveguides with large (~10 to $100~\mu m^2$) mode areas (6–10). Although such experiments using bulky discrete components have been successful in demonstrating small- and medium-scale quantum circuits, it is desirable to achieve CV quantum states with comparable qualities in nanophotonics to enable large-scale integrated quantum circuits.

In nanophotonics, silicon nitride (SiN) and silica platforms have been used for many quantum photonic experiments, such as entangled photon-pair generation, squeezing, error correction, and small-scale Gaussian boson sampling (11–13). However, their inherently weak cubic $[\chi^{(3)}]$ nonlinearity typically necessitates using high–quality factor resonators, which imposes limitations on accessible squeezing levels and bandwidths. Despite advances, the measured squeezing levels have so far remained around 2 dB in nanophotonics (see supplementary materials, section 8).

On the other hand, the measurements in CV quantum systems have typically relied on balanced homodyne detection using highly efficient and low-noise photodetectors, which are limited to bandwidths in the mega- to gigahertz range (14). Moreover, in nanophotonics, the loss associated with transferring the microscopic quantum states from a tightly confined mode to a photodetector has imposed barriers in the measurement capabilities of such states (15-17). A potential solution for these measurement challenges lies in all-optical measurement schemes based on a noiseless phase-sensitive amplifier with sufficiently large gain (18-21) that can eliminate the bandwidth limitations of homodyne detection and the sensitivity to detection losses. However, achieving such large gains (>30 dB) over broad optical bandwidths is challenging in nanophotonics with cubic nonlinearity (22). Such an all-optical measurement allows one to exploit the entire optical bandwidth of quantum fields and thereby paves a practical path toward ultrafast all-optical CV quantum information processors using time- and frequencymultiplexed schemes (6-8).

Recently, lithium niobate (LN) nanophotonics has opened promising avenues in optical communication, sensing, and computation owing to its extraordinary optical, electrical, and acoustic properties (23). A combination of subwavelength confinement of the optical mode, strong $\chi^{(2)}$ nonlinearity, high-fidelity

quasi-phase-matching by periodic poling, and dispersion engineering for longer interaction lengths has enabled devices outperforming the traditional LN devices (24–26).

In this work, we used a nanophotonic circuit in LN to experimentally demonstrate the generation and all-optical measurement of an ultra-short-pulse squeezed vacuum as the building block of scalable CV quantum nanophotonics. Our circuit combines two dispersionengineered phase-sensitive optical parametric amplifiers (OPAs) (24) (Fig. 1). The first OPA generates a microscopic squeezed vacuum, which is then amplified with a high-gain OPA to macroscopic levels within the same nanophotonic chip. The resulting macroscopic field carries information about the microscopic squeezed state, which can be measured with a high tolerance to loss.

The phase-space distributions for the vacuum (black circle) and the phase-quadrature squeezed vacuum (filled ellipse) are shown in Fig. 1A. The measurement OPA selects a certain quadrature of the microscopic squeezed field and amplifies it to macroscopic levels, in principle without adding any noise. In Fig. 1, B and C, the phase-space distributions (filled ellipses) corresponding to amplified antisqueezed and amplified squeezed quadratures are shown for two particular pump phases of the measurement OPA, ϕ_{pump2} . We set ϕ_{pump1} = 0 and use it as the phase reference for pump 2.

In the case of Fig. 1B with $\phi_{pump2} = 0$, the anti-squeezed quadrature (Q) is amplified while the orthogonal phase quadrature (P) is deamplified such that the output field is dominated entirely by the Q quadrature, and the P quadrature can be considered negligible. In such a high-gain amplification regime, the total average photon number (power) of the output field is $\langle \hat{N}_{+} \rangle \simeq \langle \hat{Q}_{\rm asq-amp}^2 \rangle \approx \mathcal{O}(10^5)$, where $\langle \hat{N}_{+} \rangle$ and $\langle \hat{Q}_{\rm asq-amp} \rangle$ denote the photon number and quadrature operators, respectively, for the amplified anti-squeezed quadrature. Likewise, by changing the pump phase of the measurement OPA to $\phi_{pump2} = \pi$, the original squeezed quadrature is amplified $\,$ to achieve $\langle \hat{N}_{-} \rangle \propto \langle \hat{P}_{\rm sq-amp}^2 \rangle \approx \mathcal{O}(10^3)$, where $\langle \hat{N}_{-} \rangle$ and $\langle \hat{P}_{\rm sq-amp} \rangle$ represent the photon number and quadrature operators, respectively, for the amplified squeezed quadrature (Fig. 1C). As a result, the macroscopic output of the measurement OPA provides a direct all-optical measurement for the quadrature variances of the microscopic squeezed state. Likewise, we determine the quadrature variances of the microscopic vacuum state by measuring the average photon number of the macroscopic amplified vacuum state when the squeezer OPA pump 1 is blocked. The phasespace distributions of the amplified vacuum are represented as the black ellipses in Fig. 1, B and C, corresponding to $\phi_{pump2} = 0$ and

¹Department of Electrical Engineering, California Institute of Technology, Pasadena, CA 91125, USA. ²Jet Propulsion Laboratory, California Institute of Technology, Pasadena, CA 91109, USA.

^{*}Corresponding author. Email: marandi@caltech.edu (A.M.); rnehra@caltech.edu (R.N.)

[†]These authors contributed equally to this work

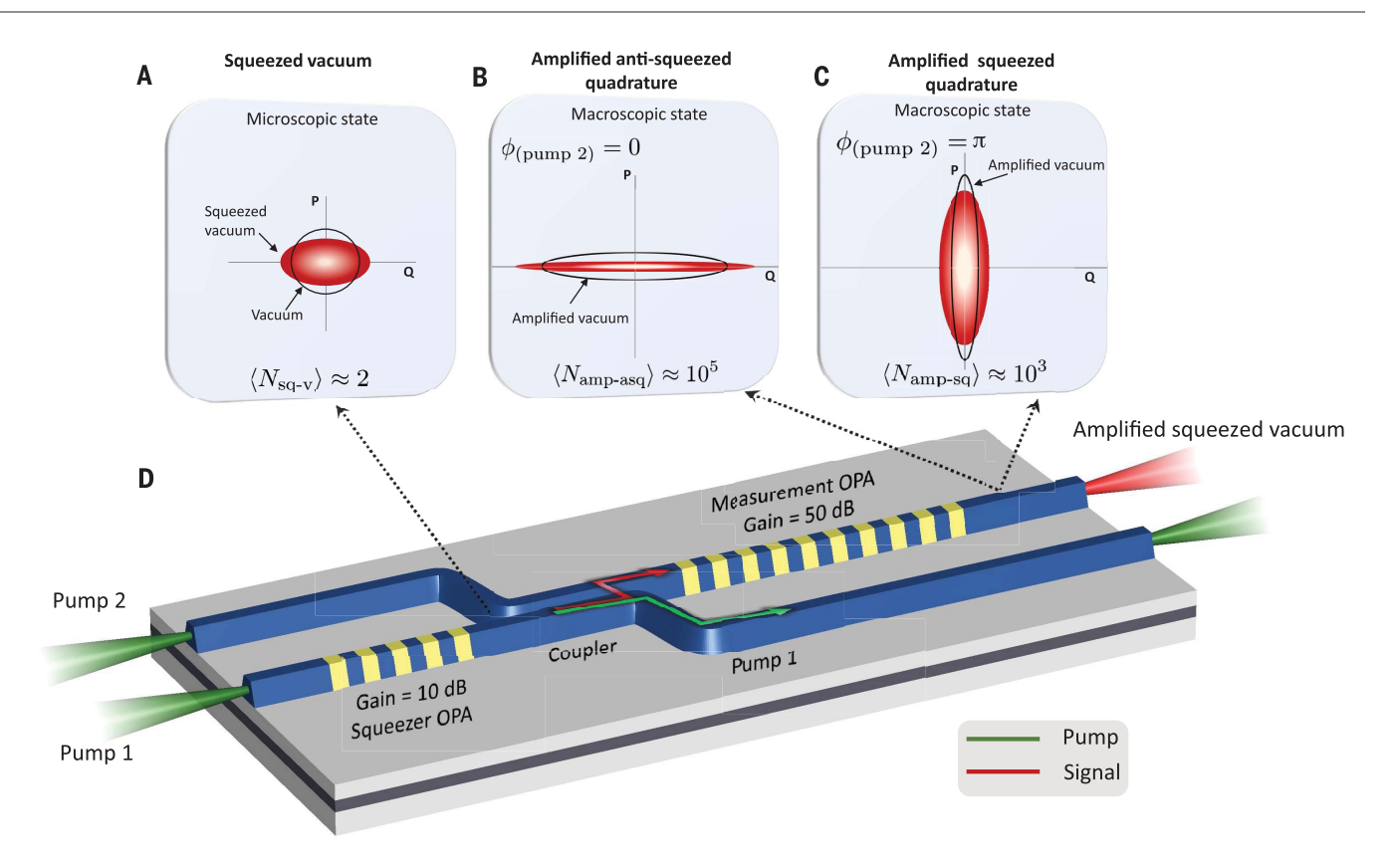


Fig. 1. Illustration of the generation of a squeezed vacuum and its all-optical measurement in nanophotonics. Phase-space distributions (filled ellipses) of (**A**) phase-quadrature squeezed vacuum, and its amplification in the (**B**) anti-squeezed and (**C**) squeezed quadratures. The black circle in (A) represents the microscopic vacuum state, and black ellipses in (B) and (C) correspond to the macroscopic vacuum state amplified in Q and P quadratures, respectively. (**D**) Sketch of our nanophotonic device consisting of the squeezer OPA, tapered adiabatic coupler, and measurement OPA. When pumped, the squeezer OPA generates a

squeezed vacuum state, which is selectively coupled into an adjacent waveguide. It is subsequently amplified by the measurement OPA to macroscopic power levels. The measurement OPA amplifies the quadrature under measurement to sufficiently above the vacuum noise, thereby making the measurement insensitive to losses due to off-chip coupling and imperfect detection. For (A), (B), and (C), we consider 10 dB of squeezing with mean photon number $\langle N_{\rm sq-v} \rangle \approx 2$, and a 50 dB phase-sensitive gain in the measurement OPA, thereby amplifying the few-photon squeezed state to a macroscopic power level.

 $\phi_{pump2}=\pi,$ respectively. The anti-squeezing (\mathcal{S}_+) and squeezing (\mathcal{S}_-) can then be determined as $S_{\pm}[dB]=10\log_{10}\left[\left\langle\hat{N}_{\pm}\right\rangle/\left\langle\hat{N}_{v_{\pm}}\right\rangle\right]$, where $\left\langle\hat{N}_{v_{+}}\right\rangle \propto \left\langle\hat{Q}_{v-amp}^2\right\rangle$ and $\left\langle\hat{N}_{v_{-}}\right\rangle \propto \left\langle\hat{P}_{v-amp}^2\right\rangle$ denote the average photon number of the vacuum state amplified in the amplitude and phase quadratures, respectively (Fig. 1, B and C).

In the ideal case, the squeezing (antisqueezing) can be determined as

$$S_{\pm}[dB] = 10\log_{10}\left[\frac{\sinh^{2}(r_{2} \pm r_{1})}{\sinh^{2}r_{2}}\right]$$
 (1)

where r_1 and r_2 are the gain parameters for the squeezer and measurement OPAs, respectively. Sufficient gain (>33 dB for ~11 dB of squeezer OPA gain; supplementary materials, section 5) in the measurement OPA allows a direct measurement of the phase-squeezed vacuum generated in the squeezer OPA. Crucially, the high-gain measurement OPA makes our measurement tolerant to off-chip coupling losses and photodetection inefficiencies as high as \sim 7 dB (supplementary materials, section 4).

In experiments, the squeezer (low-gain) and measurement (high-gain) OPAs of our circuit are periodically poled with lengths of 2.5 and 5.0 mm, respectively. The output of the squeezer OPA (microscopic squeezed vacuum) is coupled to the measurement OPA through a directional coupler. To make our directional coupler broadband and less susceptible to fabrication imperfections, we used an adiabatic design where both of the waveguides are tapered, while keeping the gap constant throughout the coupler length. The coupler directs the squeezed vacuum to the adjacent waveguide toward the measurement OPA and keeps the residual pump of the squeezer OPA in the original waveguide (Fig. 1D). The fabricated adiabatic coupler causes ~30% loss for the squeezed vacuum and leaks ~20% of the squeezer pump to the measurement OPA. Our numerical simulations suggest that the coupling performance of the adiabatic coupler can be improved to >98% for the squeezed signal and <5% for the squeezer pump with proper calibration of fabrication steps, which will lead to better measurement qualities (supplementary materials, section 4).

In our simplified experimental setup (Fig. 2A) the squeezer and measurement OPAs are pumped by a mode-locked laser (Menlo Svstems Orange A) generating ~75-fs-long nearly transform-limited pulses at a 250-MHz repetition rate. The relative phase between pump 1 (squeezer OPA) and pump 2 (measurement OPA) pulses is modulated by a piezoelectric transducer (PZT) on the pump 2 arm. At the output of the nanophotonic chip, the amplified squeezed signal and measurement OPA pump are first separated using a dichroic mirror and then are detected by two different optical spectrum analyzers (OSAs; see supplementary materials, section 1). In Fig. 2A, we show (i) a false-colored scanning electron microscope (SEM) image of our nanophotonic

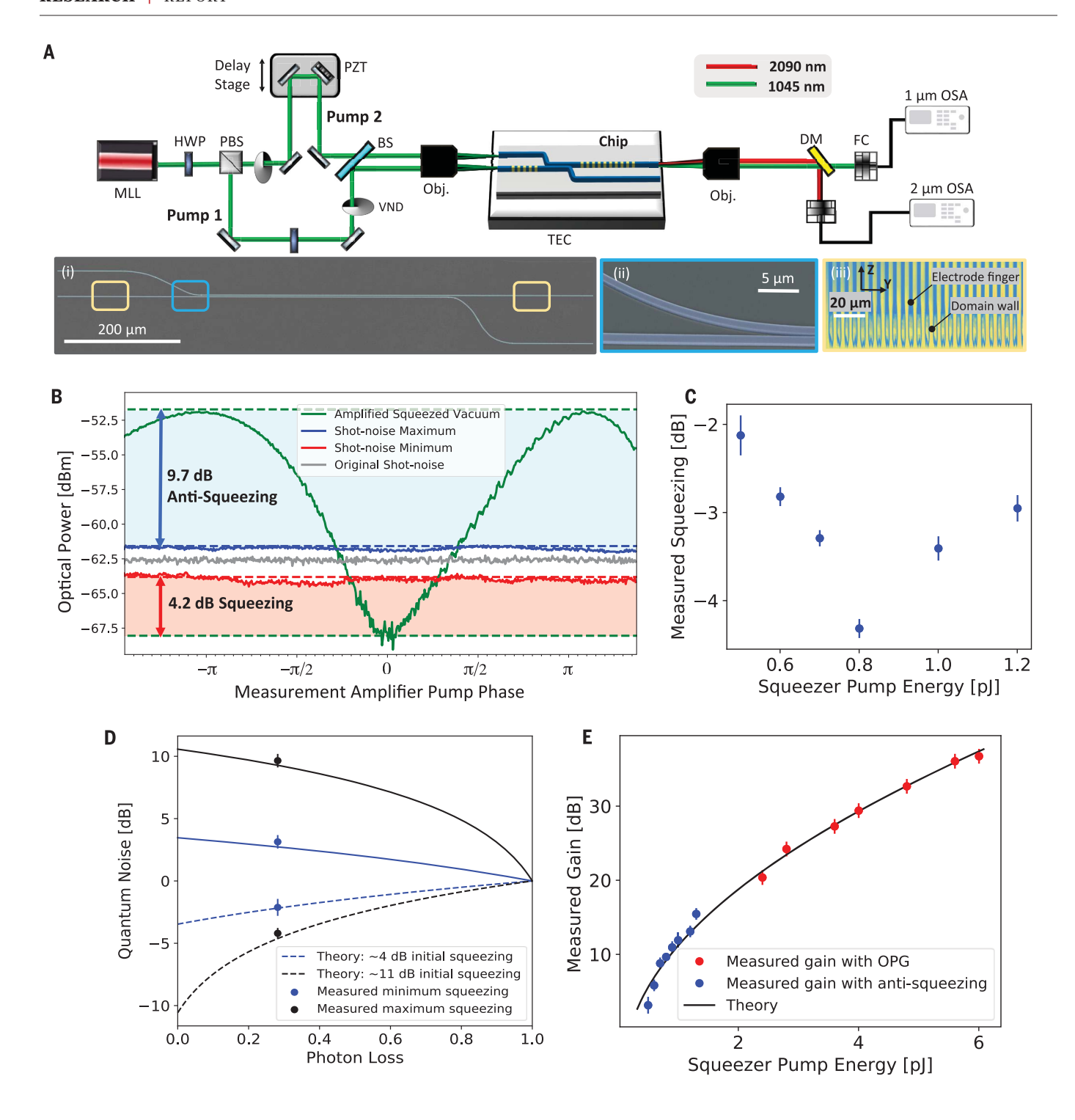


Fig. 2. Generation and measurement of squeezed light in the LN nanophotonic chip. (A) Experimental setup. A mode-locked laser (MLL) is used to pump the squeezer (pump 1) and measurement (pump 2) OPAs. At the output of the nanophotonic chip, the amplified squeezed signal (red) and residual pump 2 (green) are separated using a dichroic mirror (DM) and measured by two different OSAs. Bottom row shows the following: (i) a false-colored SEM image of our nanophotonic circuit, (ii) a zoomed-in SEM image of the coupler region, and (iii) a false-colored second harmonic microscope image of the periodically poled region before etching the waveguides. (B) Squeezing measurement by an OSA in the zero-span mode at 2090 nm. (C) The squeezing measured at

2090 nm for several values of pump 1 while keeping pump 2 constant. (**D**) Loss analysis of the squeezing measurements. The solid (dashed) curves show the degradation of anti-squeezing (squeezing) as the photon loss increases, and the solid data points correspond to measured values of minimum and maximum squeezing. (**E**) The squeezer gain dependence on the energy of pump 1. Blue points are measured from anti-squeezing, and red points are directly obtained from optical parametric generation (OPG) measurements. Error bars are obtained from the statistics of the measurements. PBS, polarized beam splitter; BS, beam splitter; HWP, half-wave plate; Obj., reflective objective; VND, variable neutral-density filter; FC, fiber coupler; TEC, thermoelectric cooler.

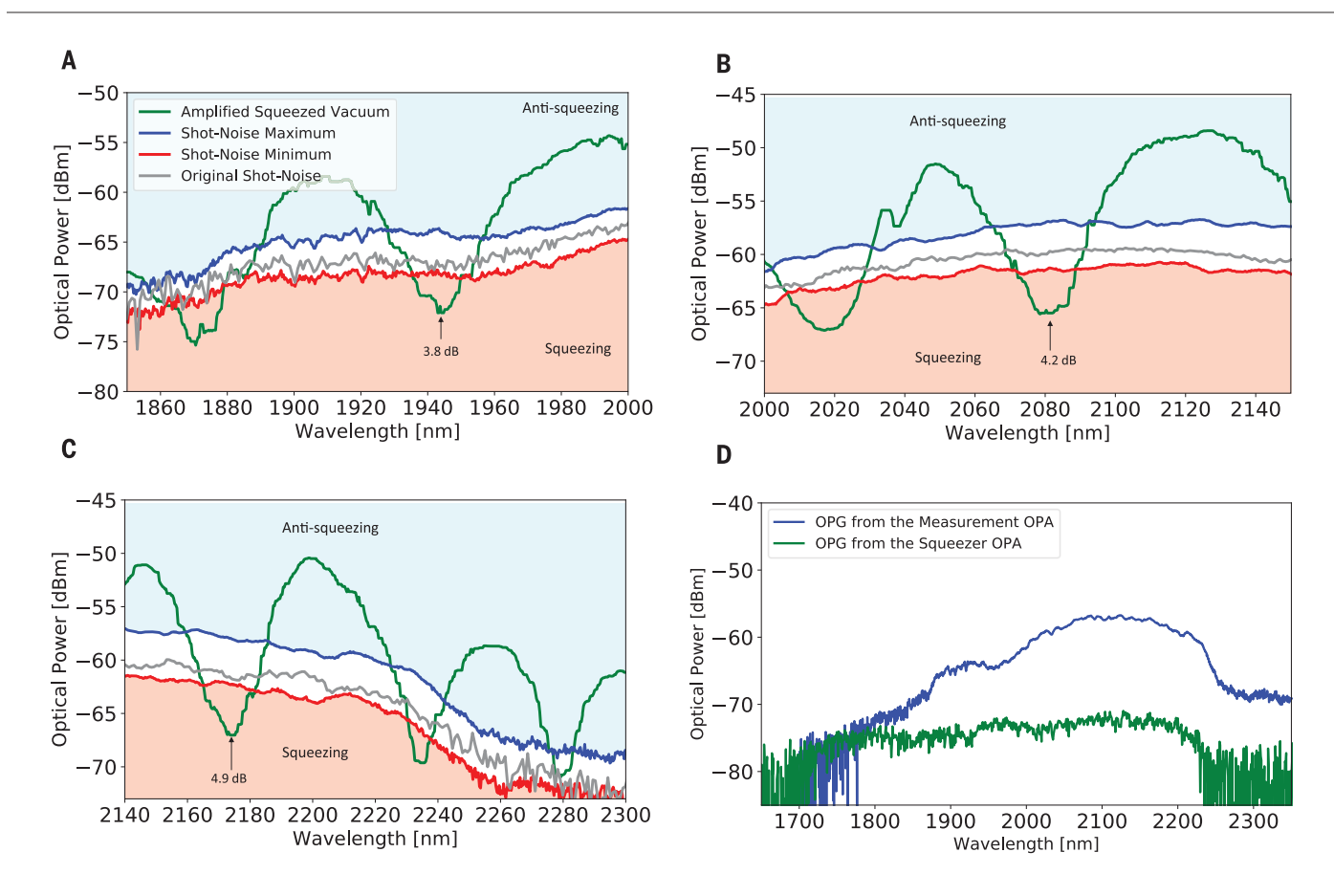


Fig. 3. Broadband squeezing measurements. (**A** to **C**) Three measurements over different selected bandwidths of the OSA when the PZT is modulated with a 300 mHz ramp signal. The shot noise traces (blue, gray, and red) were acquired with pump 1 blocked. (**D**) Optical parametric generation from the squeezer OPA (green) and measurement amplifier OPA (blue). Both traces are acquired at ~6 pJ of pulse energy.

circuit, (ii) a zoomed-in SEM image of the coupler region, and (iii) a false-colored second harmonic microscope image of the periodically poled region before etching the waveguides.

Figure 2B shows an example measurement of our squeezed state. The green trace shows the output signal of the measurement OPA using an OSA in a zero-span mode at 2090 nm while keeping both pump 1 and pump 2 on and modulating the PZT by a 1-Hz ramp signal. To accurately measure the squeezing, we need to eliminate the effect of residual interference of the two pumps at the output of the measurement. We achieve this by determining the maximum and minimum of this residual interference and then calibrating our amplified shot-noise levels by subsequently varying the power of pump 2 to these maximum and minimum pump powers while blocking pump 1. These two levels of pump 2 result in a "shot-noise maximum" and "shotnoise minimum," as shown in Fig. 2B, while the "original shot-noise" corresponds to the pump 2 level during the squeezing measurement. Hence, in the squeezing measurement, the shaded area below (above) the shot-noise minimum (shot-noise maximum) corresponds to squeezing (anti-squeezing) at the input of the high-gain OPA. We measured a squeezing and anti-squeezing level of 4.2 ± 0.2 dB and 9.7 ± 0.1 dB, respectively, with 0.8 pJ of squeezer OPA pump energy. A detailed discussion on our shot-noise calibration measurements can be found in section 2 of the supplementary materials.

We further characterize the dependence of squeezing at 2090 nm on the pump power while keeping pump 2 constant and performing the shot-noise calibration for each power level as shown in Fig. 2C. As we increase the pump power in the squeezer OPA, the level of measured squeezing increases at first. However, above 0.8 pJ of pump pulse energy, we observe that further increasing the squeezer pump decreases the level of measured squeezing. The degradation of measured squeezing at high pump powers may be due to the existence of a small phase noise and relative chirp between pump 1 and pump 2, which can mix the loss-degraded squeezed quadrature with the relatively large anti-squeezed quadrature (27). Additionally, parasitic nonlinear effects such as the photorefractive effect and nonlinear absorption mechanisms in the waveguide can also account for the degradation of squeezing at higher pump powers.

Figure 2D shows how squeezing levels degrade in the presence of photon loss $(1 - \eta)$. Analytically, $S_{+}^{\eta}[dB] = 10\log[(1-\eta) + \eta e^{\pm 2r_1}],$ where $(1 - \eta)$ determines the loss experienced by the microscopic squeezed signal and r_1 is the squeezing parameter characterizing nonlinear interaction strength (supplementary materials, section 5). The solid dots in Fig. 2C are the experimental data points for the minimum and maximum amount of measured squeezing at 2090 nm. From these measurements, we estimate the total loss $L = 1 - n \approx$ 0.3 experienced by the microscopic squeezed signal before being fully amplified by the measurement OPA. The estimated total loss is mostly dominated by the coupling efficiency of the adiabatic coupler, which we measured using an auxiliary signal centered at 2090 nm (supplementary materials, section 4). From the squeezing and anti-squeezing measurements in Fig. 2D, our inferred squeezing after correcting for losses is 10.48 ± 0.87 dB with a pump energy of <1 pJ. This paves the way for fault-tolerant CV quantum processors in LN nanophotonics, as 10.5 dB of squeezing is sufficient for many architectures, including recent proposals with Gottesman-Kitaev-Preskill qubit encodings (28).

Figure 2E depicts the gain in the squeezer OPA as a function of pump 1 pulse energy. The gain for lower pump energies (<2.4 pJ) is determined from the anti-squeezing measurements, whereas for higher pump energies (>2.4 pJ), we obtain the gain from a direct measurement of average photon number (supplementary materials, section 4). When there is no input seed into the measurement OPA, the average number of photons in the high parametric gain regime $(\langle \hat{N} \rangle \sim G/4)$ allows us to estimate the gain. The solid curve is the fit that includes the overall detection efficiency (including off-chip coupling losses and imperfect detection after the measurement OPA) and the nonlinear strength as fitting parameters. From the fit, we extract the overall detection efficiency of $\eta_{overall}^{off-chip} \sim 0.20$ (supplementary materials, section 5). This level of linear loss puts an upper limit of <1 dB to the measurable squeezing for a standard balanced homodyne detection. This is not a limiting factor for our all-optical squeezing measurements, because of the noiseless amplification by the measurement OPA. Note that such lossy measurements are even more detrimental for highly squeezed states, as they are extremely sensitive to losses. This can be seen in Fig. 2D, where ~11 dB of initial squeezing degrades by ~10 dB in the presence of the detection losses of $L_{
m overall}^{
m off-chip} =$ $1 - \eta_{\text{overall}}^{\text{off-chip}} = 0.80$. However, our all-optical measurement is not affected by $L_{\text{overall}}^{\text{off-chip}}$ losses owing to the amplification by the measurement OPA and allows us to measure the squeezing levels as high as 4.9 dB. Thus, our current measured squeezing is mostly limited by the coupling loss associated with the onchip adiabatic coupler, which can reach with near unity coupling efficiencies through better calibration of fabrication steps, as suggested by our numerical simulations (supplementary materials, section 4).

Figure 3, A to C, shows the measured squeezing over a broad bandwidth. The amplified shot-noise is calibrated, using the same method as discussed earlier, over the entire spectrum. Green traces correspond to measurements by the OSA over three different spectral windows when the PZT is modulated by a slow ramp signal at 300 mHz. Squeezing is present over the entire spectrum, with a slight spectral dependence. The measured squeezing is 3.8 ± 0.4 dB around 1950 nm. 4.2 ± 0.2 dB around 2090 nm. and

 4.9 ± 0.2 dB around 2200 nm. The slight spectral dependence is attributed to the wavelength dependence of the coupling efficiency of our adiabatic coupler (supplementary materials, section 4). We measured the squeezing bandwidth to be 25.1 THz. The bandwidth is expected to increase to 36.4 THz, as confirmed by the optical parametric generation (OPG) from the squeezer OPA in Fig. 3D. The measured squeezing bandwidth is mostly limited by the slight mismatch of measurement OPA gain in the wings of the spectrum, as evident from its OPG signal. Because of this difference in the gain spectrum, the measurement OPA does not amplify the squeezed vacuum over its entire generation bandwidth to macroscopic levels, leading to a reduced measured squeezing bandwidth. These measurements indicate that our generated squeezed state can occupy a record-level time window of about four optical cycles (supplementary materials, section 3). This temporal window can be shortened further by engineering the dispersion and quasi-phase matching (29) and may lead to opportunities for studying quantum fields in the extremely short-pulse regime (30). Our demonstrated squeezing bandwidth allows the definition of few-optical-cycle temporal bins in time-multiplexed CV quantum information processors (6, 7). As a result, such ultra-short time bins can be defined in a dense manner for which centimeter-scale on-chip delay lines can be used for large-scale cluster states on a chip.

We have demonstrated few-cycle vacuum squeezing and its all-optical measurements in the LN nanophotonic platform. Our on-chip all-optical loss-tolerant broadband measurements through high-gain phase-sensitive amplification enabled squeezing measurements over more than 25 THz of bandwidth while providing measurement purification against the detection losses as high as $L_{\rm overall}^{\rm off-chip} \sim 7$ dB. Combined with the recent advances such as high-speed electro-optic modulators and integrated single-photon detectors (23), we envision that our results may enable scalable ultrafast all-optical quantum information processors in LN nanophotonic platform.

REFERENCES AND NOTES

- 1. T. D. Ladd et al., Nature 464, 45-53 (2010).
- J. L. O'Brien, A. Furusawa, J. Vučković, Nat. Photonics 3, 687–695 (2009).
- 3. H. Yu et al., Nature **583**, 43-47 (2020).
- 4. C. A. Casacio et al., Nature 594, 201-206 (2021).
- A. Furusawa et al., Science 282, 706–709 (1998).
- W. Asavanant et al., Science 366, 373–376 (2019).

- M. V. Larsen, X. Guo, C. R. Breum, J. S. Neergaard-Nielsen, U. L. Andersen, Science 366, 369–372 (2019).
- M. Chen, N. C. Menicucci, O. Pfister, *Phys. Rev. Lett.* 112, 120505 (2014).
- 9. G. Kanter et al., Opt. Express 10, 177-182 (2002).
- J. Roslund, R. M. De Araujo, S. Jiang, C. Fabre, N. Treps, Nat. Photonics 8, 109–112 (2014).
- 11. V. D. Vaidya et al., Sci. Adv. 6, eaba9186 (2020).
- 12. C. Vigliar et al., Nat. Phys. 17, 1137-1143 (2021).
- 13. J. M. Arrazola et al., Nature **591**, 54–60 (2021).
- 14. J. F. Tasker et al., Nat. Photonics 15, 11–15 (2021).
- 15. U. A. Javid et al., Phys. Rev. Lett. 127, 183601 (2021).
- 16. P.-K. Chen, I. Briggs, S. Hou, L. Fan, Opt. Lett. 47, 1506–1509
- 17. D. Peace et al., arXiv:2204.05694 [quant-ph] (2022).
- 18. C. M. Caves, Phys. Rev. D 26, 1817-1839 (1982)
- 19. Y. Shaked et al., Nat. Commun. 9, 609 (2018).
- 20. N. Takanashi *et al.*, *Opt. Express* **28**, 34916–34926
- 21. G. Frascella, S. Agne, F. Y. Khalili, M. V. Chekhova, NP.J. Ouantum Inf. 7, 72 (2021).
- 22. Z. Ye et al., Sci. Adv. 7, eabi8150 (2021)
- 23. D. Zhu et al., Adv. Opt. Photonics 13, 242 (2021).
- 24. L. Ledezma et al., Optica 9, 303 (2022).
- 25. M. Jankowski et al., Optica 7, 40 (2020).
- 26. Y. Hu et al., Nature 599, 587-593 (2021).
- M. J. Werner, M. G. Raymer, M. Beck, P. D. Drummond, Phys. Rev. A 52, 4202–4213 (1995).
- 28. J. E. Bourassa et al., Quantum 5, 392 (2021).
- 29. D. Horoshko, M. Kolobov, Phys. Rev. A 88, 033806 (2013).
- 30. M. Kizmann et al., Nat. Phys. 15, 960-966 (2019).
- 31. R. Nehra, Few-cycle vacuum squeezing in nanophotonics, Figshare (2022); https://doi.org/10.6084/m9.figshare.20100140.v1.

ACKNOWLEDGMENTS

The device nanofabrication was performed at the Kavli Nanoscience Institute (KNI) at Caltech. The authors thank NTT Research for financial and technical support. The authors thank C. González-Arciniegas and O. Pfister for fruitful discussions. Funding: The authors gratefully acknowledge support from ARO grant W911NF-18-1-0285, NSF grants 1846273 and 1918549, AFOSR award FA9550-20-1-0040, and NASA/JPL. This project was funded in part by the President's and Director's Research and Development Fund of Caltech and JPL. Author contributions: R.N. and A.M. conceived of the idea and designed the experiments; R.N. designed the devices with assistance from L.L. and Q.G.; R.S. fabricated the devices and L.L. performed the periodic poling; R.N. carried out the experiments with assistance from R.S., R.M.G., O.G., and A.R.; R.N. performed the theoretical and numerical analysis with contributions from L.L.: R.N. and A.M. wrote the manuscript with input from all other authors; and A.M. supervised the project. Competing interests: R.N., A.M., R.S., and L.L. are inventors on a provisional patent application (63/299,762) by the California Institute of Technology based on the work presented here. Data and materials availability: All other data needed to evaluate the conclusions in the paper are present in the paper or the supplementary materials. The data files supporting the plots in the main text are available at Figshare (31). License information: Copyright © 2022 the authors, some rights reserved; exclusive licensee American Association for the Advancement of Science. No claim to original US government works. https://www.science.org/ about/science-licenses-journal-article-reuse

SUPPLEMENTARY MATERIALS

science.org/doi/10.1126/science.abo6213 Materials and Methods Figs. S1 to S13 Table S1 References (32–50)

Submitted 15 February 2022; accepted 8 August 2022 10.1126/science.abo6213